INTERNATIONAL JOURNAL OF
INFORMATION AND SYSTEMS SCIENCES
Volume 1, Number 2, Pages 120–136

APPLICATION OF MULTIRESOLUTION ANALYSIS TO DIRECTION-OF-ARRIVAL ESTIMATION

YANBO XUE, JINKUAN WANG, AND XIN SONG

Abstract. This paper provides a comprehensive investigation of applications of the subband decomposition theory to the direction-of-arrival (DOA) estimation problem, which is one of the key problems in array signal processing. The superiorities of subband decomposition are given and, particularly, the merits of subband spectra like signal-to-noise ratio (SNR) and frequency spacing widening are analyzed. Combined with the MUSIC and the ESPRIT methods, subband-based MUSIC (SB-MUSIC) and subband-based ESPRIT (SB-ESPRIT) are suggested, along with the modified version of SB-ESPRIT, namely non-mapping back SB-ESPRIT. The respective simulation results related to each method show that the subband-based methods outperform the ones which estimate directly the fullband signals.

Key Words. Array signal processing, subband, DOA, MUSIC, ESPRIT

1. Introduction

High-resolution methods of direction-of-arrival (DOA) estimation have been a topic of great importance in recent years for their wide-spread applications in radar, sonar, and mobile communication [7, 8]. Recently, most multiple source detection techniques are based on the eigenstructure decomposition of the covariance matrix. Among them, MUltiple SIgnal Classification (MUSIC) method [13] and Estimation of Signal Parameter via Rotational Invariance Technique (ESPRIT) [12] have been widely used for DOA estimation, harmonic analysis, frequency estimation, delay estimation, and the combinations thereof. Both approaches are implemented on the basis of a fixed, uniform, spatial sampling for all signal directions, which show the possibility of performance enhancement if a multiresolution signal representation is introduced [19].

Subband decomposition is a technique to split the spectrum of fullband signal with bandpass filters and subsampling to have a time-frequency decomposition, which provides a candidate to multiresolution method. Rao and Pealman proved in [11] that with subband decomposition, some superiorities can be obtained comparing with the direct estimation on the fullband signal. Classical wavelet transform (WT) [10] is a two-subband decomposition method, which presents the resolution both in frequency domain and time domain. Different mother wavelets are designed to deal with different scenarios. Wavelet packet (WP) is a much detailed WT by decomposing the *approximations* and *details* as well. Wavelet-based method for array processing has been studied by many researchers. The early successful application

Received by the editors February 21, 2005 and, in revised form, March 22, 2005.
This research is supported by Key Program of Science and Technology from the Ministry of Education of China, under Grant no. 02085, and Education Bureau of Hebei Province of China, Science Research Directive Plan no. Z2004103.

of WT and WP is in harmonic retrieval [9, 2]. Recently, the application of wavelet theory in DOA estimation problem has become the interest of many researchers [15, 21, 20].

Inspired by the work of [9] and [15], a novel subband-based method for DOA estimation (SB-MUSIC) is proposed in this paper by combining subband decomposition with MUSIC. Wavelet packet is chosen to decompose the subbands for its capability of *details*-decomposition, which provides a solution to the problem in [15]. The proposed method is performed by wavelet packets decomposition of the signal, using a minimum description length (MDL) criterion [16] as the guidance of each decomposition . A best bases method (BBM) [3] is employed to choose the best bases of the WP tree . MUSIC method is applied to all the best bases, yielding all the DOAs. The proposed method provides both savings of computation and improvement of resolution, which is a good candidate of foremost preprocessing method for many DOA estimation algorithms and even for TAM and SSM to refine the performance, especially in scenarios of low signal-to-noise ratio (SNR) and closely spaced spatial frequency. In the case of the low computational load of ESPRIT, a subband-based ESPRIT (SB-ESPRIT) method is proposed in this paper. When coherent signals imping, SB-ESPRIT can decorrelate them by decomposing them into different subbands. The SB-ESPRIT, in essence, is a beamspace approach [1, 18].

Though SB-ESPRIT works well in most cases, SB-ESPRIT has two major problems related to its implementation and performance. First, the method requires a procedure to map the subband spatial frequency back to the fullband. This manipulation is necessary because of the widening of the spatial frequency spacing [14]. Second, the reduction of computational load in the singular value decomposition (SVD) is achieved at the expense of compromising the output SNR. A modified SB-ESPRIT algorithm for DOA estimation is also suggested in this paper. The proposed method is based on the pre-expansion of the sensor array such that the mapping back manipulation after the estimation of bearings is no longer required. The modified SB-ESPRIT first expands the array, and then uses SB-ESPRIT to decompose the fullband signal into several subbands. The combination of ESPRIT estimates at each subband yields the fullband bearings, which is guaranteed by the pre-expansion of the array. The rotational invariance of our proposed method is proven.

2. Problem formulation

Throughout this paper, we consider a Uniform Linear Array (ULA) with K isotropic sensors spaced by a distance d. D ($D < K$) narrowband plane waves imping from the far-field with the same center frequency ω_0, which is shown in Figure 1. The bearings of the D signals are denoted by $\theta_1, \theta_2, \cdots, \theta_D$. The received data sampled at the k-th sensor can be expressed as

$$x_k(n) = \sum_{i=1}^{D} s_i(n) \mathrm{e}^{-j\omega_0(k-1)\sin\theta_i d/c} + w_k(n). \tag{1}$$

In matrix form, we have

$$\mathbf{x}(n) = \mathbf{A}\mathbf{s}(n) + \mathbf{w}(n), \tag{2}$$

where $\mathbf{x}(n)$, $\mathbf{s}(n)$, and $\mathbf{w}(n)$ denote respectively the $K \times 1$ received data vector, the $D \times 1$ wavefront vector, and the $K \times 1$ additive noise vector, which are given by

$$\mathbf{x}(n) = [x_1(n), x_2(n), ..., x_K(n)]^{\mathrm{T}},$$

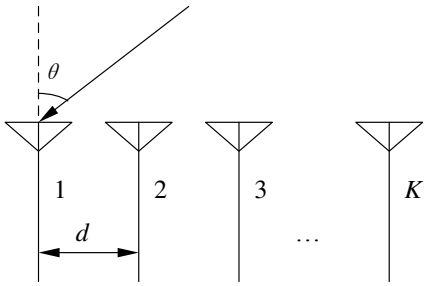

FIGURE 1. Uniform linear array

$$\mathbf{s}(n) = [s_1(n), s_2(n), ..., s_D(n)]^{\mathrm{T}},$$
$$\mathbf{w}(n) = [w_1(n), w_2(n), ..., w_K(n)]^{\mathrm{T}}.$$

Define $\omega_i = \omega_0 \sin\theta_i d/c$ as the equivalent spatial frequency of the i-th wavefront. Then, the mixing matrix $\mathbf{A} \in \mathcal{C}^{K\times D}$ can be expressed as

$$\mathbf{A}(\omega) = [\mathbf{a}(\omega_1), \mathbf{a}(\omega_2), \cdots, \mathbf{a}(\omega_D)], \tag{3}$$

where $\mathbf{a}(\omega_i) = [1, \mathrm{e}^{-j\omega_i}, \cdots, \mathrm{e}^{-j(K-1)\omega_i}]^{\mathrm{T}}$ denotes the steering vector corresponding to the spatial frequency ω_i, and superscript T stands for transpose. (1) can be rewritten as

$$x_k(n) = \sum_{i=1}^{D} s_i(n)\mathrm{e}^{-j(k-1)\omega_i} + w_k(n), \tag{4}$$

where $s_i(n) = |s_i(n)|\mathrm{e}^{-j\phi_i}$ is the complex source waveform, where the phase ϕ_i is uniformly distributed over $[0, 2\pi)$. Assume that the signals are zero mean wide sense stationary (WSS) processes, and $w_k(n)$ is the zero mean white Gauss noise (WGN) which is uncorrelated to the signals and has identical variance σ^2 in each sensor. From the above assumptions, the autocorrelation function of the k-th signal is given by

$$R_{xx}(k) = \sum_{i=1}^{D} P_i \mathrm{e}^{-j(k-1)\omega_i} + \sigma^2\delta(k) \tag{5}$$

where $P_i := |s_i|^2$ denotes the power of the i-th signal and $\delta(k)$ is the Dirac function.

Theorem 1. *(*Spatial Shannon Theorem*) For signals with the same wavelength and received by the sensor array, there is no aliasing of the spectrum if we ensure that the baseline space is not larger than a half wavelength, that is $d \le \lambda/2$, where λ denotes wavelength of the signal.*

Proof. Take a ULA for example, if we locate the sensors along the time axis, the outputs can be taken as the samples of the spatial signals with an equal interval, where the sampling frequency is $\omega_0 = 2\pi$. It is required in the Shannon sampling theorem that the maximal frequency of the signals should not be larger than half of the sampling frequency to prevent the aliasing, which is formulated by

$$\max\{\omega_i\} = \max\{2\pi \cdot \sin\theta_i \cdot \frac{d}{\lambda}\} \le \frac{\omega_0}{2}. \tag{6}$$

Solving (6) yields the relationship $d \le \lambda/2$. The proof of Theorem 1 is completed. □

Usually we choose the baseline space $d = \lambda/2$ to satisfy the Spatial Shannon Theorem. In this case, we have that $\omega_i = \pi \sin\theta_i \in [-\pi, \pi]$.

3. Subband decomposition

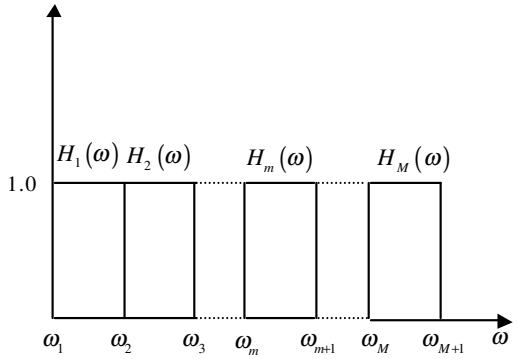

FIGURE 2. Ideal bandpass filters for M subbands

Subband decomposition deals with the fullband source by bandpass filtering and subsampling its spectrum to obtain the decomposition in frequency domain. The ideal bandpass filters for M subbands are given in Figure 2. Although this technique introduces delay into real-time system, this drawback is offset by the superiorities gained from processing subband signal rather than the fullband signal [11]. Subband decomposition theory is first brought forward by Crochiere [4] to have speech coding and fully analyzed by Rao and Pealman in [11]. The obvious gains have made subband decomposition applicable in compression of video, image, audio and speech data [17, 6].

3.1. Superiorities of subband decomposition. Rao and Pealman have proven in [11] that some superiorities can be obtained by dealing with the subband signals upon fullband signal, which are concluded in the following aspects.

(1) The aggregate of the minimum prediction error of the subbands is less than that of the fullband signal.
(2) For Gaussian source, the composite entropies of the subbands are closer to the entropy rate of the source than that of the fullband.
(3) The spectral flatness measure (SFM) of the Gaussian source is less than that of the subbands, which means that the SFM of the subbands is much flatter.

Besides that, subband decomposition for spatial frequency estimation in this paper has two advantages: not only are the various modes isolated in separate subbands, but also the SNR and spatial frequency spacing are doubled in each two-subbands' splitting. It is well known that the Cramer-Rao bound (CRB) of the estimation goes better if there is smaller number of modes in each subband.

3.2. SNR amplification and spatial frequency spacing widening. Two key features of subband signals, named SNR amplification and spatial frequency spacing widening, are given by Tkacenko and Vaidyanathan in [14]. They have formed the basic advantages of application of subband decomposition in array signal processing.

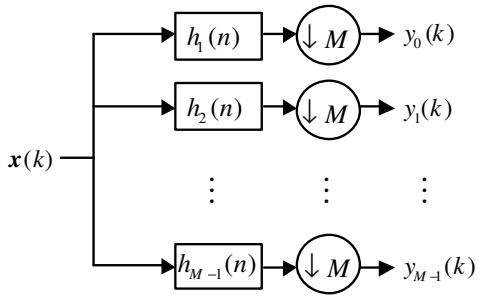

FIGURE 3. M band filter bank

We suppose that the signal $x(k)$ is input to a bank of ideal bandpass filters shown in Figure 3, where $\downarrow M$ means to decimate the fullband signal by a ratio M. Then, the m-th ($m = 1, 2, \cdots, M$) subband is given by

$$y_m(k) = \sum_{i=1}^{D} s_i H_m(\mathrm{e}^{-j\omega_i})\mathrm{e}^{-j(m-1)\tilde{\omega}_{i,m}} + w_m(k), \tag{7}$$

where $w_m(k)$ denotes the additive noise process seen in the m-th subband. $\tilde{\omega}_{i,m}$ denotes frequency of the i-th subband in the m-th subband and is given by

$$\tilde{\omega}_{i,m} = \begin{cases} M\omega_i - (m-1)\pi\mathrm{sgn}(\omega), & m = 1, 3, 5, \cdots \\ M\omega_i - m\pi\mathrm{sgn}(\omega), & m = 2, 4, 6, \cdots \end{cases} \tag{8}$$

It can be easily verified that by filtering the WGN $w(k)$ with variance σ^2 by means of an identity filter $\left[|H_m(\mathrm{e}^{-j\omega})|^2\right]_{\downarrow M} = 1$, the noise $w_m(k)$ is also WGN with variance σ^2. To this end, we suppose that

$$|H_m(\mathrm{e}^{-j\omega})|^2 = \begin{cases} M, & \omega \in I_m, \\ 0, & \text{otherwise}, \end{cases} \tag{9}$$

where I_m denotes the frequency range of the m-th subband and is given by

$$I_m = \left[\frac{(m-1)\pi}{M}, \frac{m\pi}{M}\right) \bigcup \left(-\frac{m\pi}{M}, -\frac{(m-1)\pi}{M}\right] \tag{10}$$

with

$$\bigcup_{m=1}^{M} = [-\pi, \pi], \quad I_m \bigcap I_n = \phi, m \neq n. \tag{11}$$

Then the autocorrelation of the subband signal $y_m(k)$ is given by

$$R_{y_m y_m}(k) = \sum_{i=1}^{D} P_i |H(\mathrm{e}^{-j\omega_i})|^2 \mathrm{e}^{j(k-1)\tilde{\omega}_{i,m}} + R_{w_m w_m}(k). \tag{12}$$

From (5), the SNR of the i-th signal in the fullband is

$$\mathrm{SNR}_{i,fb} = \frac{P_i}{\sigma^2}. \tag{13}$$

Substituting (9) into (12), we have

$$\begin{aligned} R_{y_m y_m}(k) &= \sum_{\omega_i \in I_m} MP_i \mathrm{e}^{j(k-1)\tilde{\omega}_{i,m}} + R_{w_m w_m}(k) \\ &= \sum_{i=1}^{D_m} \tilde{P}_{i,m} \mathrm{e}^{j(k-1)\tilde{\omega}_{i,m}} + \sigma^2 \delta(k), \end{aligned} \tag{14}$$

where D_m denotes the number of signals in the subband signal $y_m(k)$, $\tilde{P}_{i,m} = MP_i$ denotes the power of the i-th signal in the m-th subband. Hence, the SNR of the i-th signal in the m-th subband is

$$\mathrm{SNR}_{i,sb} = \frac{\tilde{P}_{i,m}}{\sigma^2} = M \cdot \mathrm{SNR}_{i,fb}, \tag{15}$$

and so the SNR of individual signal is amplified by a factor of M.

Next we consider the case that there are two spatial frequencies $\omega_p, \omega_q \in I_m$ in the fullband. For simplicity, we suppose that both of them are positive frequencies. Then they can be expressed as

$$\omega_p = \frac{m\pi}{M} + \beta_p, \quad \omega_q = \frac{m\pi}{M} + \beta_q, \tag{16}$$

where $0 \leq \beta_p, \beta_q < m\pi/M$. The frequency spacing between ω_p and ω_q in the fullband is $\Delta\omega_{fb} := |\omega_p - \omega_q| = |\beta_p - \beta_q|$. From (8) we have their counterpart frequencies $\tilde{\omega}_{p,m}$ and $\tilde{\omega}_{q,m}$ in the m-th subband. It is easy to show that the spacing between $\tilde{\omega}_{p,m}$ and $\tilde{\omega}_{q,m}$ is

$$\Delta\omega_{sb} := M|\beta_p - \beta_q| = M \cdot \Delta\omega_{fb} \tag{17}$$

no matter which subband are they in, and so the frequency spacing is widened by a factor of M.

4. Subband-based DOA estimation method

4.1. Subband-based MUSIC method. For computation's sake, a pseudo-2D method is suggested in this paper. Pseudo-2D means to decompose each snapshot of the ungrouped signal matrix by wavelet packets while keeping the number of snapshots unchanged. After all the snapshots are decomposed all the *approximations* and *details* are regrouped into two matrices for next-level decomposition. Pseudo-2D method is performed with the supervision of minimum description length criterion and the decomposed wavelet packets tree is also pruned by the best base method. The following is a summary of SB-MUSIC method based on the signal model (2).

Step 1: Take snapshots of signal model (2) and form an $K \times N$ matrix $\mathbf{X} = [\mathbf{x}(1), \mathbf{x}(2), ..., \mathbf{x}(N)]$, where $\mathbf{x}(i), i = 1, 2, ...N$, is defined in (2).

Step 2: Perform pseudo-2D method on $\mathbf{X}$ and yield the *approximation* $\mathbf{X}_1$ and *detail* $\mathbf{X}_2$.

Step 3: Apply MDL criterion to the mother node $\mathbf{X}$ and its children nodes $\mathbf{X}_1$ and $\mathbf{X}_2$, respectively. If there are no modes lost, accept two nodes and go to **Step 2** for next decomposition. Otherwise, stop the decomposition at node $\mathbf{X}$.

Step 4: Prune the decomposed tree by BBM.

Step 5: Apply MUSIC method to all the leaves to obtain the estimates of the corresponding subbands.

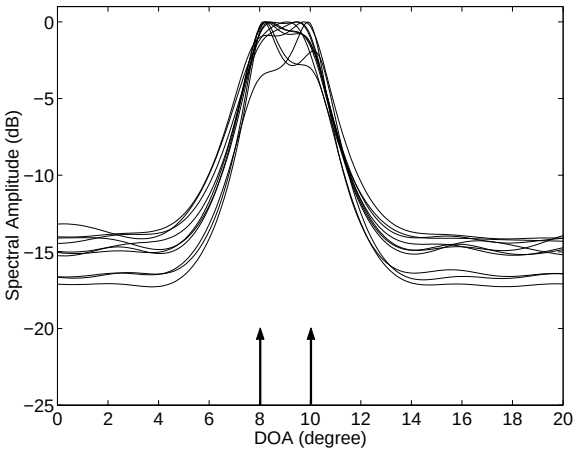

FIGURE 4. MUSIC spatial spectrum for two signals with equal power (SNR = -5 dB) from 8° and 10° by ten batches.

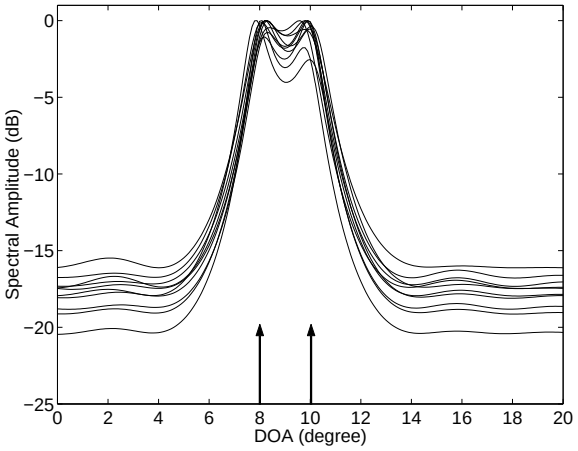

FIGURE 5. SB-MUSIC spatial spectrum for two signals with equal power (SNR = -5 dB) from 8° and 10° by ten batches.

It is also worth noting that the SB-based DOA estimation method is not confined to the classical algorithm. The proposed method focuses on the algorithm itself. The goal is to increase the estimation of resolution at low SNR and the small number of snapshots, and to reject the noise by more detailed decomposition. To generalize the SB-based DOA estimation methods, other high resolution algorithms, such as ML, ESPRIT, and MEM, can be used.

The computation loads of classical MUSIC method consist of two main parts, the decomposition of matrix ($\mathcal{O}(K^3)$) and the searching for the peaks ($\mathcal{O}(D^3)$), where K and D are the numbers of sensors and plane waves, respectively. The computational advantage of SB-MUSIC is that it reduces the number of sensors to its half, and only adds a small amount of computation loads of wavelet packet transform. For the one-level D_1 wavelet packets decomposition, the added computation loads are only $\mathcal{O}(K)$. Even for the l-level, the added computation loads are about $\mathcal{O}(K) +$

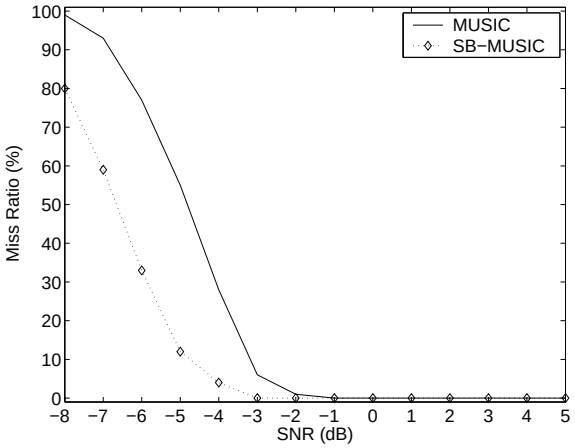

FIGURE 6. Miss Ratio of MUSIC and SB-MUSIC vs. SNR for two signals from 8° and 10°.

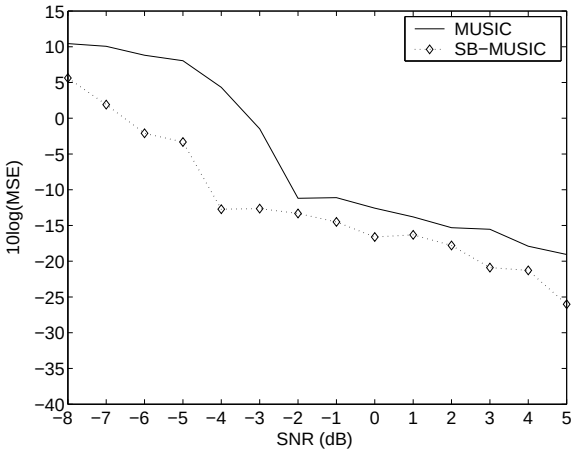

FIGURE 7. 10log(MSE) of MUSIC and SB-MUSIC vs. SNR for two signals from 8° and 10°.

$2\mathcal{O}(2^{-1}K) + ... + 2^{l-1}\mathcal{O}(2^{-l+1}K)$. The computation superiority of SB-MUSIC is obvious with easy validation.

Next we present some simulations to justify the performance of proposed SB-MUSIC algorithm and compare it with classical MUSIC algorithm. In both examples, simulations are carried out according to signal model (2) for a half wavelength spaced ($d = \lambda/2$) ULA with 32 sensors ($K = 32$), and the number of snapshots taken from the array is 100 ($N = 100$). The mother wavelet used for SB-MUSIC method is Daubechies' D_1 wavelet (the same as Haar wavelet) for computations' saving [5].

In the example, the low SNR case (SNR = -5 dB) is considered. Two plane waves at closely spaced directions 8° and 10° with equal power are impinging on the array. Suppose that we have an one-level wavelet packets decomposition and two subbands yielded. By applying ten batches to the MUSIC and SB-MUSIC method, we obtain the spatial spectrums shown in Figures. 4 and 5, respectively. Five ones

miss presenting two dominant peaks corresponding to the DOAs of the two waves in ten batches with the classical MUSIC method, while all ten batches resolve two DOAs with SB-MUSIC method. The capability of closed DOA resolving at low SNR and small number of snapshots owes to the spatial frequency spacing and SNR amplification. Figures 6 and 7, presenting the performance of SB-MUSIC (the diamond dashed line) upon classical MUSIC (the solid line) in the sense of miss ratio and MSE versus SNR, are depicted by 100 Monte Carlo simulations. The superiorities of resolution enhancing and noise rejecting of the supposed method are obvious.

4.2. Subband-based ESPRIT method. ESPRIT has advantages over another widely used MUSIC [13] method because, compared to MUSIC, ESPRIT requires lower computational burden by exploiting the rotational invariance between two subarrays. However, ESPRIT experiences significant performance degradation when the SNR is low. The performance becomes even poorer when coherent signals imping.

The idea of SB-ESPRIT is to first partition the measured data into several subbands and then apply the ESPRIT algorithm to each subband. For the convenience of analysis, we define two matrices $\mathbf{H}$ and $\mathbf{G}$, both of dimension $N_f \times K$, to filter the measured data, described in (2), into a low frequency subband and a high frequency subband, where $N_f = \lfloor (K + N_d)/2 \rfloor - 1$ with N_d denoting the length of filter and $\lfloor y \rfloor$ denoting the largest integer not exceeding y. The output of the two filters are formulated by

$$\mathbf{x}_h(n) = \mathbf{HAs}(n) + \mathbf{w}_h(n) \tag{18}$$

and

$$\mathbf{x}_g(n) = \mathbf{GAs}(n) + \mathbf{w}_g(n), \tag{19}$$

where $\mathbf{x}_h(n)$ and $\mathbf{x}_g(n)$, both of dimension $N_f \times 1$, are referred to as the low frequency and high frequency data vectors. Each of them can be used to compose two subarrays. Taking $\mathbf{x}_h(n)$ for example, we choose its 1st to $(N_f - 1)$th rows to form the vector $\mathbf{x}_h^1(n)$ corresponding to the first subarray, whereas its 2nd to N_fth rows are used to form vector $\mathbf{x}_h^2(n)$ corresponding to the second subarray.

For simplicity, we choose Haar wavelets as the analysis filters and assume K is even so that $K/2$ is an integer. The 1-level lowpass and highpass filtering matrices $\mathbf{H}$ and $\mathbf{G}$ are given, respectively, by

$$\mathbf{H} = c \cdot \begin{bmatrix} \mathcal{J}_2 & O_2 & \cdots & O_2 \\ O_2 & \mathcal{J}_2 & \cdots & O_2 \\ \vdots & \vdots & \ddots & \vdots \\ O_2 & O_2 & \cdots & \mathcal{J}_2 \end{bmatrix} \in \mathcal{R}^{K/2 \times K} \tag{20}$$

and

$$\mathbf{G} = c \cdot \begin{bmatrix} \mathcal{K}_2 & O_2 & \cdots & O_2 \\ O_2 & \mathcal{K}_2 & \cdots & O_2 \\ \vdots & \vdots & \ddots & \vdots \\ O_2 & O_2 & \cdots & \mathcal{K}_2 \end{bmatrix} \in \mathcal{R}^{K/2 \times K}, \tag{21}$$

where $\mathcal{J}_2 = [1, 1]$, $\mathcal{K}_2 = [1, -1]$, $O_2 = [0, 0]$, and $c = 1/\sqrt{2}$.

Next we exploit the rotational invariance between subarrays. Denote the $K/2 \times D$ mixing matrix at the high frequency subband by

$$\tilde{\mathbf{A}} = \mathbf{HA} = \begin{bmatrix} \tilde{\mathbf{a}}_1 & \tilde{\mathbf{a}}_2 & \cdots & \tilde{\mathbf{a}}_D \end{bmatrix} \tag{22}$$

where

$$\tilde{\mathbf{a}}_i = \left(1 + \mathrm{e}^{-j\omega_i}\right) \begin{bmatrix} 1 & \mathrm{e}^{-j2\omega_i} & \cdots & \mathrm{e}^{-j(K-2)\omega_i} \end{bmatrix}^{\mathrm{T}}. \tag{23}$$

Then, (18) can be rewritten as

$$\mathbf{x}_h(n) = \tilde{\mathbf{A}}\mathbf{s}(n) + \mathbf{w}_h(n). \tag{24}$$

If the first subarray consists of the 1st to the $(K/2-1)$th sensors and the second subarray consists of the 2nd to the $K/2$th sensors, the mixing matrices $\tilde{\mathbf{A}}_1$ and $\tilde{\mathbf{A}}_2$ of two subarrays can then be related by a diagonal matrix Φ, i.e., $\tilde{\mathbf{A}}_2 = \tilde{\mathbf{A}}_1\Phi$, where Φ is the rotational invariance in the subband signals, given by

$$\Phi = \mathrm{diag}\{\mathrm{e}^{-j2\omega_1}, \mathrm{e}^{-j2\omega_2}, \cdots, \mathrm{e}^{-j2\omega_D}\}. \tag{25}$$

The rotational invariance property between two subarrays is evident because they undergo the same lowpass filtering. The same can be said for the subarrays corresponding to the high frequency subband. By exploiting the diagonal elements of Φ using conventional ESPRIT, we can obtain the spatial frequency $\tilde{\omega}_{l,m}$ in the subbands without knowing the mixing matrix $\tilde{\mathbf{A}}_1$, where $\tilde{\omega}_{l,m}$ means the subband frequency obtained at the lth-level and mth-node. So the validity of SB-ESPRIT is shown with a 1-level Haar wavelet decomposition. The extension to an *any-level any-type* wavelet decomposition is straightforward. Note that the subband frequency is amplified in Φ, which accords with the superiority of frequency widening.

To obtain the fullband frequencies, we need to map the frequencies from subbands back to the fullband. We map the frequencies as follows:

$$\omega_{fb} = \begin{cases} \dfrac{\tilde{\omega}_{l,m} + (m-1)\pi \mathrm{sgn}(\tilde{\omega}_{l,m})}{2^l}, & m = 1, 3, 5, \cdots \\ \dfrac{\tilde{\omega}_{l,m} - m\pi \mathrm{sgn}(\tilde{\omega}_{l,m})}{2^l}, & m = 2, 4, 6, \cdots \end{cases} \tag{26}$$

where $\mathrm{sgn}(\tilde{\omega}_{l,m})$ denotes the sign of $\tilde{\omega}_{l,m}$. Then it is easy to obtain the DOAs from

$$\theta_i = \arcsin\left\{\frac{\omega_{i,fb} \cdot c}{\omega_0 \cdot d}\right\} = \arcsin\left\{\omega_{i,fb} \cdot \frac{\lambda}{d}\right\}. \tag{27}$$

Now we give the summary of the SB-ESPRIT algorithm based on TLS criterion:

Step 1: Form the matrix $\mathbf{X} = [\mathbf{x}(1), \mathbf{x}(2), \cdots, \mathbf{x}(N)]$ by taking N snapshots of model (2).

Step 2: Filter $\mathbf{X}$ with wavelet packet filters $\mathbf{H}$ and $\mathbf{G}$ to yield two matrixes $\mathbf{X}_h = \mathbf{H}\mathbf{X}$ and $\mathbf{X}_g = \mathbf{G}\mathbf{X}$.

Step 3: Determine the number of signals by applying the minimum description length (MDL) criterion to the mother node $\mathbf{X}$ and its two children nodes $\mathbf{X}_h$ and $\mathbf{X}_g$. Accept the children nodes and go to **Step 2** if there are no modes lost. Otherwise stop the decomposition at the mother node.

Step 4: Prune the binary tree using the best bases method to find the optimal leaf nodes.

Step 5: Divide each leaf nodes into two subarrays and apply TLS-ESPRIT to estimate the subband spatial frequency $\tilde{\omega}_{l,m}$.

Step 6: Map the subband frequency $\tilde{\omega}_{l,m}$ back to the fullband frequency $\omega_{i,fb}, i = 1, 2, \cdots, D$, using (26), and then the DOAs from (27).

Next, we give computer simulations to compare the SB-ESPRIT with standard ESPRIT algorithm. Both simulations are carried out for a half wavelength ($d = \lambda/2$) spaced ULA with $K = 32$ isotropic sensors. Four sources emitting narrowband signals with the same power, and propagating in distinct directions with DOAs $10^\circ, 20^\circ, 40^\circ$, and 60° are considered. The number of snapshots taken from the array

is $N = 100$ and the Haar wavelet packets are chosen as the subband decomposition filters. We use Monte-Carlo simulation method to have 100 runs of each example. In the first example, a very low SNR scenario is chosen to evaluate the performance of SB-ESPRIT and ESPRIT in high power interference scenarios. Figure 8(a) and Figure 8(b) illustrate the estimated DOAs with the standard ESPRIT and SB-ESPRIT algorithm for $\theta = 10°, 20°, 40°$, and $60°$ with SNR $= -13$ dB and 100 trial runs. We notice that the estimates with SB-ESPRIT are closely distributed along the DOAs, while those with ESPRIT are not. Figure 9 shows the resulting root mean square error (RMSE) of the estimated DOAs as a function of SNR. SB-ESPRIT algorithm outperforms ESPRIT especially at low SNR for its ability of SNR amplification in the subbands. The second example depicts the decorrelation ability of SB-ESPRIT algorithm compared with the standard ESPRIT, as shown in Figure 10. The RMSE is greatly decreased with the growth of SNR.

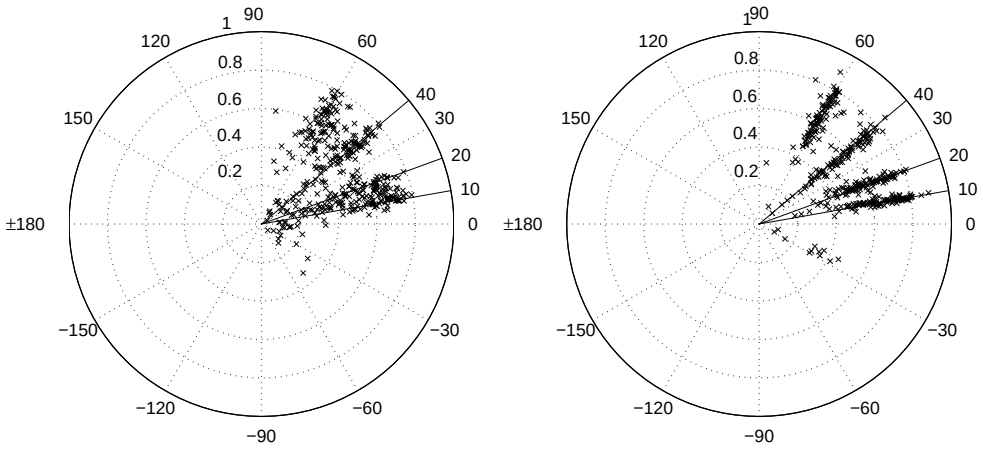

(a) ESPRIT (b) SB-ESPRIT

FIGURE 8. Estimates with the standard ESPRIT algorithm for $\theta = 10°, 20°, 40°$, and $60°$ with SNR $= -13$ dB and 100 trial runs.

4.3. Non-mapping back SB-ESPRIT method. Because the spatial frequency spacing is widened in each-level decomposition [14], we need to map the frequency in the subband back to the fullband by using (26). Here, we propose a pre-expansion method to circumvent this procedure. Take the Haar wavelet as an example, and the distance between sensors is doubled after each level of decomposition, which is the key principle for multiresolution estimation of the signal [19]. It is the spatial widening property that requires the mapping back manipulation (26). The idea of pre-expansion method is to modify the received matrix before it is input to the wavelet filters. The pre-expansion matrix $\mathbf{P}$ is defined as follows:

$$\mathbf{P} = \begin{bmatrix} 1 & & \\ & \tilde{\mathbf{P}} & \\ & & 1 \end{bmatrix} \in \mathcal{R}^{K_p \times K}, \tag{28}$$

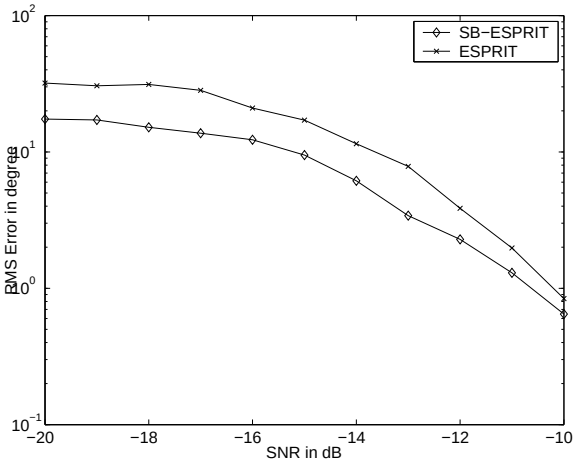

FIGURE 9. RMSE of the estimated DOAs as a function of SNR for $\theta = 10°, 20°, 40°$, and $60°$ (cross line - ESPRIT, diamond line - SB-ESPRIT).

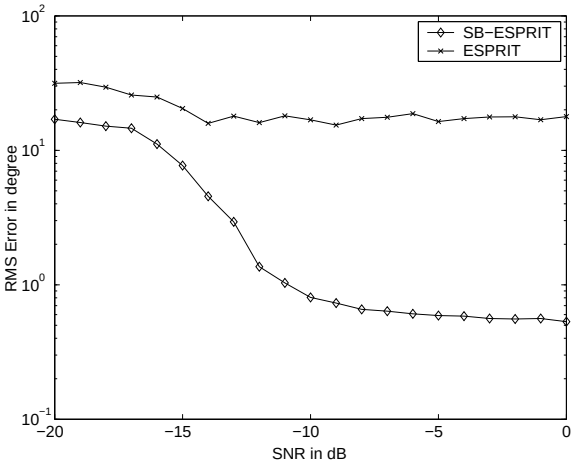

FIGURE 10. RMSE of the estimated DOAs as a function of SNR for two uncorrelated DOAs $20°$ and $60°$, and two correlated DOAs $10°$ and $40°$ (cross line - ESPRIT, diamond line - SB-ESPRIT)

where $K_p = 2(K-1)$ is the number of virtual expanded array and $\tilde{\mathbf{P}}$ is given by

$$\tilde{\mathbf{P}} = \begin{bmatrix} \mathcal{J}_2 & O_2 & \cdots & O_2 \\ O_2 & \mathcal{J}_2 & \cdots & O_2 \\ \vdots & \vdots & \ddots & \vdots \\ O_2 & O_2 & \cdots & \mathcal{J}_2 \end{bmatrix}^{\mathrm{T}} \in \mathcal{R}^{(2K-4)\times(K-2)}.$$

Expanding (2) with (28) yields

$$\mathbf{x}_p(n) = \mathbf{PAs}(n) + \mathbf{w}_p(n). \tag{29}$$

It is easy to verify that $\mathbf{w}_p(n)$ is also WGN with variance σ^2. SB-ESPRIT can also be applied to the expansion matrix, while we should prove the rotational variance after expanding and filtering the matrix.

Suppose we filter $\mathbf{x}_p(n)$ with a lowpass Harr filter $\mathbf{H} \in \mathcal{R}^{(K-1)\times 2(K-1)}$ as in (18). We obtain

$$\mathbf{x}_{ph}(n) = \check{\mathbf{A}}\mathbf{s}(n) + \mathbf{w}_{ph}(n), \tag{30}$$

where $\check{\mathbf{A}} = \mathbf{HPA}$ denotes the $(K-1) \times D$ subband matrix

$$\check{\mathbf{A}} = \begin{bmatrix} \check{\mathbf{a}}_1 & \check{\mathbf{a}}_2 & \cdots & \check{\mathbf{a}}_D \end{bmatrix} \tag{31}$$

with $\check{\mathbf{a}}_i = [1 + \mathrm{e}^{-j\omega_i}, \mathrm{e}^{-j\omega_i} + \mathrm{e}^{-j2\omega_i}, \cdots, \mathrm{e}^{-j(K-2)\omega_i} + \mathrm{e}^{-j(K-1)\omega_i}]^{\mathrm{T}}$.

Let the first subarray consist of the 1st to $(K-2)$th sensors and the second subarray consist of those from 2nd to $(K-1)$th. The rotational invariance still holds between the subband mixing matrices $\check{\mathbf{A}}_1$ and $\check{\mathbf{A}}_2$, given by

$$\check{\Phi} = \mathrm{diag}\{\mathrm{e}^{-j\omega_1}, \mathrm{e}^{-j\omega_2}, \cdots, \mathrm{e}^{-j\omega_D}\}, \tag{32}$$

which is the same as the conventional ESPRIT and does not require mapping back manipulation after the subband frequency is estimated. Our proposed non-mapping back method can be also easily implemented by adding a step called *pre-expansion* before applying SB-ESPRIT algorithm.

The applicability of SB-ESPRIT in coherent signals scenario is not to decorrelate the coherent signals by averaging the subarray autocorrelation matrix, but to decompose them into different subbands. Given ideal bandpass filters and appropriate division schedule, decorrelation is realized.

Next, we provide computer simulations to evaluate and compare the performance of conventional ESPRIT, SB-ESPRIT, and the modified SB-ESPRIT. Both simulations are carried out for a ULA of $K = 32$ isotropic sensors with half wavelength ($d = \lambda/2$) interelement spacing. Four sources emit narrowband signals with the same power from 10°, 20°, 60° and 70°. Among them, the two signals from 10° and 60° are coherent. $N = 100$ snapshots are taken and the Haar wavelet packets are chosen as the subband decomposition filters. We use the Monte-Carlo method to obtain 100 independent runs for each example. Figure 11 shows the performance at a low SNR = −13 dB. It is evident from Figure 11(a) that the conventional ESPRIT fails to resolve the coherent signals from 10° and 60°, whereas Figure 11(b) and Figure 11(c) show that both SB-ESPRIT and our proposed method resolve the four sources. It is also noted that the output power of modified SB-ESPRIT is obviously stronger than that of SB-ESPRIT. Figure 12 shows the resulting RMSE of the estimated DOAs as a function of SNR. SB-ESPRIT and the modified SB-ESPRIT algorithm outperform ESPRIT especially at low SNR for their ability of dividing coherent signals into different subbands. The RMSEs of the subband-based methods, which include the SB-ESPRIT and our proposed method, are significantly lower than that of conventional ESPRIT, especially when the SNR is high. In this case, the performance of the modified SB-ESPRIT and that of SB-ESPRIT become very close.

5. Conclusion

This paper has dealt with the applications of wavelets and subband decomposition to array signal processing, especially the direction-of-arrival estimation problem. The superiorities of subband decomposition are first given, and then the merits of subband spectra like SNR and frequency spacing widening are analyzed. Combined with the MUSIC and ESPRIT methods, subband-based MUSIC (SB-MUSIC) and subband-based ESPRIT (SB-ESPRIT) are suggested, along with the modified version of SB-ESPRIT, namely non-mapping back SB-ESPRIT. The proposed methods estimate the spatial frequencies by decomposing the signal into

several subbands. All of the methods are based on the Shannon Spatial Theorem. The rotational invariance holds in both SB-ESPRIT and modified SB-ESPRIT. The respective simulation results related to each method show that the subband-based methods outperform the ones which estimate directly the fullband signals.

Acknowledgments

The authors thank Prof. Yimin Zhang at the Center for Advanced Communications of Villanova University for his valuable suggestions to the amendment of the SB-ESPRIT method and its modified version. All the anonymous reviewers are thanked for their meaningful work.

References

[1] K. M. Buckley and X. L. Xu, Spatial-spectrum estimation in a location sector, *IEEE Trans. Acoust. Speech Signal Proc.*, 38 (1990), 1842–1852.

[2] Y. Chu, W. Fang, and S. Chang, An efficient Haar wavelet-based approach for the harmonic retrieval problem, *Proceedings of ICASSP97*, Münich, Germany, pp. 1969–1972, 1997.

[3] R. Coifman and M. Wickerhauser, Entropy-based algorithms for best basis selecition, *IEEE Trans. on Info. Theo.*, 38 (1992), 713–718.

[4] R. E. Crochiere, S. M. Webber, and J. K. L. Flanagan, Digital coding of speech in sub-bands, *BSTJ*, 55 (1976), 1069–1085.

[5] I. Daubechies, Orthonormal bases of compactly supported wavelets, commun. *Pure Appl. Math.*, XLI (1988), 969–996.

[6] A. Gersho, Advances in speech and audio compression, *Proce. of the IEEE*, 82 (1994), 900–918.

[7] L. C. Godara, Application of antenna arrays to mobile communications, Part II: Beam-Forming and Direction-of-Arrival Considerations, *Proceeding of IEEE*, 85 (1997), 1195–1245.

[8] H. Krim and M. Viberg, Two decades of array signal processing, *IEEE Signal Processing Magazine*, 13 (1996), 67–94.

[9] C. B. Lambrecht and M. Karrakchou, Wavelet packets-based high-resolution specttral estimation, *Signal Processing*, 47 (1995), 135–144.

[10] S. Mallat, A Wavelet Tour of Signal Processing (Second Edition), *Academic Press*, 1999.

[11] S. Rao and W. A. Pearlman, Analysis of linear prediction, coding, and spectral estimation from subbands, *IEEE Trans. Infor. Theor.*, IT-42 (1996), 1160–1178.

[12] R. H. Roy, ESPRIT-Estimation of Signal Parameters via Rotational Invariance Technique, *Ph.D Dissertation*, Stanford University, 1987.

[13] R. O. Schmidt, Multiple emitter location and signal parameter estimation, *IEEE Trans. Antennas Propag.*, Vol. AP-34, no. 3, pp. 276–280, March 1986.

[14] A. Tknacenko and P. P. Vaidyanathan, The role of filter banks in sinusoidal frequency estimation, *J. Franklin Inst.*, 338 (2001), 517–547.

[15] B. H. Wang, Y. L. Wang, and H. Chen, Spatial wavelet transform preprocessing for direction of arrival estimation, *Antennas and Propagation Society International Symposium*, 4 (2002), 672–675.

[16] M. Wax and T. Kailath, Detection of signals by information theoritic criteria, *IEEE Trans. on Acous. Speec. Signl. Proce.*, 33 (1985), 387-392.

[17] J. W. Woods, Subband Image Coding, *Kluwer Acamedic Publishers*, 1991.

[18] G. Xu, S. D. Silverstein, R. H. Roy, and T. Kailath, Beamspace ESPRIT, *IEEE Trans. Signal Proces.*, 42 (1994), 349–356.

[19] W. Xu and W. K. Stewart, Multiresolution-signal direction-of-arrival estimation: a wavelets approach, *IEEE Signal Proces. Letters*, 7 (2000), 66–68.

[20] Y. B. Xue, Wavelet Domain Multiresolution Array Signal Processing, *M.S. Dissertation*, Northeastern University of China, Shenyang, Feb. 2004.

[21] Y. Zhang and Z. H. Feng, Direction-of-arrival estimation with wavelets based spatial filtering, *Proc. of Interna. Confer. on Mircowave and Millimeter Wave Tech.*, pp. 687–690, 2000.

Yanbo Xue was born in Henan, China, in 1979. He received the B.S. degree in automation engineering from the Northeastern University in China in 2001 and M.S. degree in control theory and control engineering at the same university in 2004. Since September 2004, he has been working for his Ph. D. degree at the Northeastern University. His research interests include MIMO wireless system, wavelet-based array signal processing, time-frequency analysis, direction-of-arrival estimation, beamforming theory, and advanced control theory.

Mr. Xue received the 2001 Excellent Undergraduate Award, the 2003 Rockwell Automation Prize for Excellent Graduate, and the 2004 International Symposium on Antennas and Propagation (ISAP'04) Young Scientist Travel Grant (YSTG) held at Sendai in Japan.

Jinkuan Wang received the M. Eng. degree from the Northeastern University, Shenyang, China, in 1985, and the Ph.D. degree from the University of Electro-Communications, Japan, in 1993. As a special member, he joined the Institute of Space and Astronautical Science, Japan, in 1990. And he worked as a engineer in Research Department of COSEL company, Japan, in 1994. He is currently a professor in the School of Information Science and Engineering at Northeastern University, China, since 1998. His main interests are in the area of intelligent control and adaptive array.

Prof. Wang received the 1986 Advancement Prize of Science and Technology of Liaoning Province, China, and the 1993 PAACS Friendship Award of IEICE, Japan.

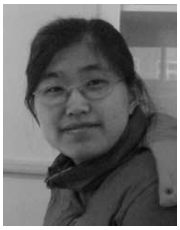

Xin Song was born in 1978, in Jilin, China. She received the B.S. degree in automation engineering from the Northeastern University in China in 2002 and M.S. degree in control theory and control engineering at the same university in 2005. Her research interests include direction-of-arrival estimation and adaptive beamforming, particularly robust adaptive beamforming.

Ms. Song received the 2004 Jian Long Scholarship for Excellent Graduate.

School of Information Science & Engineering, Northeastern University, Shenyang 110004, China
E-mail: yxue@mail.neuq.edu.cn
URL: http://www.neuq.edu.cn/sasp/ybxue

School of Information Science & Engineering, Northeastern University, Shenyang 110004, China
E-mail: wjk@mail.neuq.edu.cn
URL: http://www.neuq.edu.cn/sasp/jkwang

School of Information Science & Engineering, Northeastern University, Shenyang 110004, China
E-mail: sxin78916@mail.neuq.edu.cn
URL: http://www.neuq.edu.cn/sasp

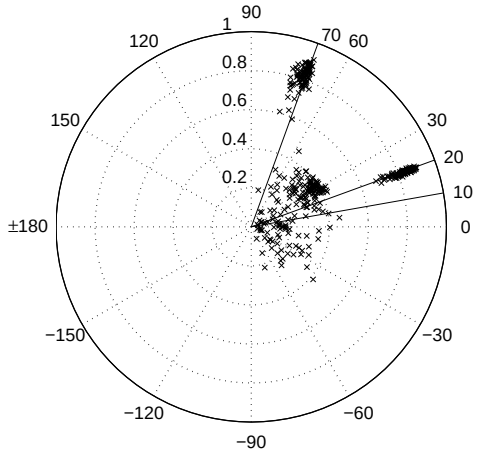

(a) ESPRIT

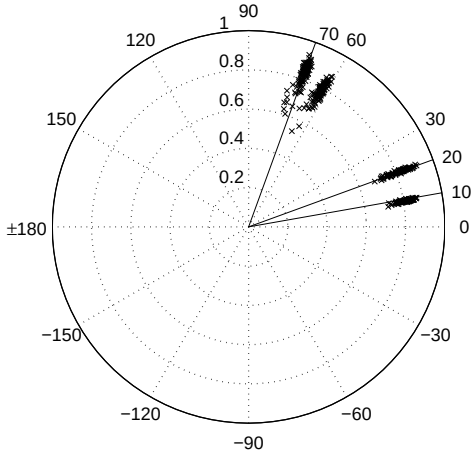

(b) SB-ESPRIT

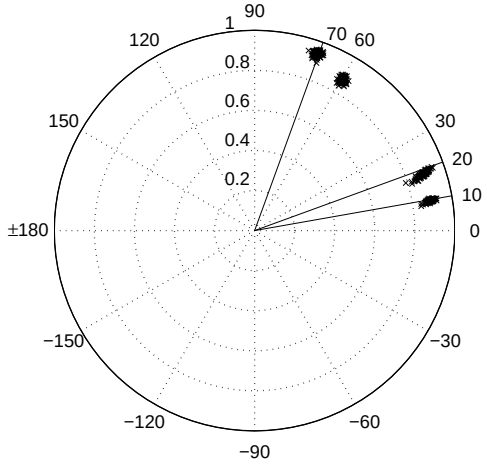

(c) ModifiedSB-ESPRIT

FIGURE 11. DOA Estimation for two coherent signals from 10° and 60°, and two incoherent signals from from 20° and 70° with SNR = −10 dB and 100 trial runs.

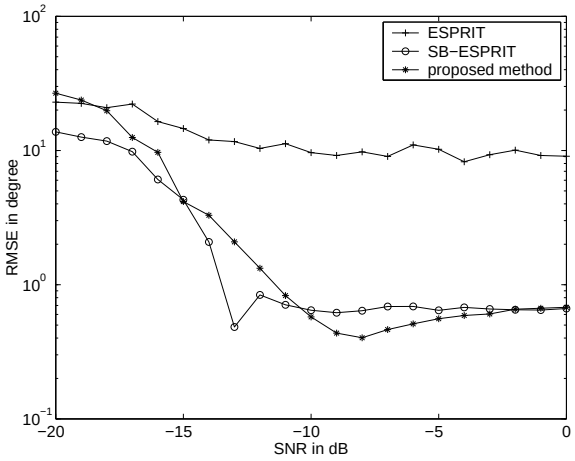

FIGURE 12. RMSE of the estimated DOAs as a function of SNR for $\theta = 10^\circ, 20^\circ, 60^\circ$, and 70°.